PHYSICAL REVIEW A VOLUME 32, NUMBER 6 DECEMBER 1985

Laser-driven shock-wave studies using optical shadowgraphy

F. Amiranoff,* R. Fedosejevs,† R. F. Schmalz, R. Sigel, and Yung-lu Teng‡
Max-Planck-Institut für Quantenoptik, D-8046 Garching, Federal Republic of Germany

(Received 29 March 1985)

The propagation of laser-induced shock waves in a transparent solid (Plexiglass) is investigated by optical shadowgraphy. The shock waves are generated by concentrating 100-J, 300-ps laser pulses from the Asterix-III iodine laser ($\lambda = 1.3$ μm) onto areas 85 or 450 μm in diameter on the target surface—this corresponding to laser irradiances of 3×10^{15} and 2×10^{14} W cm^{-2}, respectively. It is observed that the initial phase of shock-wave propagation is obscured by an electrical breakdown phenomenon, being particularly strong at the smaller laser spot size. The possible cause of this phenomenon is discussed, and it is pointed out that the field strengths of 10^8–10^9 V/m required for breakdown are generated as a consequence of charge separation during two-dimensional plasma expansion. The shock-wave trajectories observed at subsequent times are compared with one- and two-dimensional numerical simulations. Good agreement is found when the same input data as for the simulations of previous thin-foil acceleration experiments are used.

I. INTRODUCTION

When solid material is irradiated by an intense laser beam, a hot and dense plasma is formed on the irradiated surface. This plasma exerts a considerable pressure upon the neighboring material, ranging up to $\cong 100$ Mbar for present-day lasers. As is well known, the potential of pulsed lasers to generate such high pressures is being exploited in the most prominent application, namely laser fusion. But there is also a more general interest in the laser as a tool for studying the physics of high energy density.[1]

In this study we are interested in measuring the pressure exerted by the laser-heated plasma by observing the shock wave which forms in the solid material. From mass and momentum conservation the pressure p behind the shock front is related to the shock velocity v_s and the density ρ_0 (density of solid) and ρ_1 (density of compressed solid) by

$$p = \rho_0 v_s^2 (1 - \rho_0/\rho_1) . \tag{1}$$

Determination of the pressure thus requires in principle, besides the accurately known initial density ρ_0, measurement of the shock-front velocity v_s and the density ratio ρ_0/ρ_1. Especially for strong shock waves with $\rho_1 \gg \rho_0$, however, measurement of the shock-front velocity alone can give a good estimate of the pressure, in particular if the change in density is corrected for (as is done in the simulations described in this paper) by using realistic equation-of-state data.

In an early experiment laser-driven shock waves in solid targets were observed by optical shadowgraphy in our laboratory.[2,3] A Nd-glass laser delivering 12-*J*, 5-ns pulses yielded pressures of 2 Mbar in solid hydrogen and 4 Mbar in Plexiglass. However, with the low-energy, long-pulse laser available at that time it was necessary to focus the laser to a very small spot size ($\cong 40$ μm diam) in order to achieve pressures in the megabar range. The flow of the expanding plasma and the shape of the shock wave therefore strongly deviated from planar geometry; this greatly complicated quantitative comparison of the results with theoretical predictions. It was concluded at that time that more powerful lasers would be needed to produce planar shock waves. Not only would this facilitate comparison with theory, but it would also eventually make laser-driven shock waves a quantitative tool of high-pressure physics.

Indeed, with the progress made during the last few years in laser technology, the interest in laser-driven shock waves has increased. Several laboratories have reported experimental investigations of shock-wave propagation in various materials.[4–7] At our laboratory interest in laser-driven shock waves was revived when the Asterix-III iodine laser became available for target experiments. This laser delivers a 100–200-J pulse lasting 300 ps [full width at half maximum (FWHM)]. With such a laser the focal spot can be made relatively large and yet afford a still high irradiation intensity. It thus becomes possible to generate shock waves in planar geometry. As will be discussed below in more detail, with the Asterix-III laser planar conditions can be realized up to intensities of about 10^{14} W cm^{-2}.

The experiments reported here were made during an extended series of experiments on thin-film acceleration.[8] In these experiments the pressure generated on the irradiated foil surface was determined by observing the foil motion by high-speed shadowgraphy. It seemed desirable to make an independent measurement of the pressure by replacing the foil by a transparent solid target and measuring the shock-wave velocity in it. A definite advantage of this latter method is that a shock wave represents a sharp discontinuity whose position should be detectable without ambiguity. In the case of thin-foil acceleration preheating may lead to expansion of the foil material during acceleration; under certain conditions the measured velocity of the rear boundary of the foil may thus depend on the wavelength used for shadow photography and differ from the center-of-mass velocity of the foil. Besides this immediate interest in a comparative measurement of the pressure, we hoped to gain during this study more experience with laser generation of planar shock waves for future studies of problems of high-pressure physics.

Experimental observations of laser-driven shock-wave propagation in a Plexiglass target will be presented in Sec. II. Unfortunately, as we shall see, observation of the shock wave was found to be severely disturbed by a hitherto unobserved phenomenon, namely electrical breakdown in the Plexiglass in a volume underneath the focal spot. Owing to the breakdown the Plexiglass in this volume became opaque to the dye-laser light used for shadowgraphy; as a consequence, the shock wave could be observed only after traversal of the opaque region, i.e., at times where the laser pulse had already terminated. As the breakdown phenomenon became very important for our investigations, Sec. III is devoted to a discussion of its possible cause. In Sec. IV we compare the measured shock-wave trajectories during the later, observable phase with numerical simulations in one and two dimensions. In Sec. V the results are summarized and discussed.

II. EXPERIMENTAL ARRANGEMENT AND RESULTS

The basic scheme of the irradiating laser beam, the solid Plexiglass target, and the dye-laser beam used for shadowgraphy is shown in Fig. 1. The scheme is the same as previously used for such investigations.[2,3]

The target was irradiated by the Asterix-III iodine laser, described in detail elsewhere.[9] Under typical operating conditions it delivered a 100-J pulse, 280(±60) ps (FWHM) in duration, at a wavelength of 1.3 μm. The beam was focused with an $f/2$ ($f=40$ cm) aspheric lens. In the plane of smallest cross section of the focused beam 50% of the incident energy was contained in a circle 85 μm in diameter.

The experiments described below were performed with the front surface of the target in one of two positions. One position corresponded to the plane of smallest beam cross section (called "in focus"); the average intensity in this plane was 3×10^{15} W cm^{-2}. The other position (called "out of focus") was located 1 mm away (towards the laser) from the plane of smallest cross section. The average intensity in this plane was typically 2×10^{14} W cm^{-2} over an irradiated area of 450 μm in diameter. Details of the intensity distribution are given in Ref. 8.

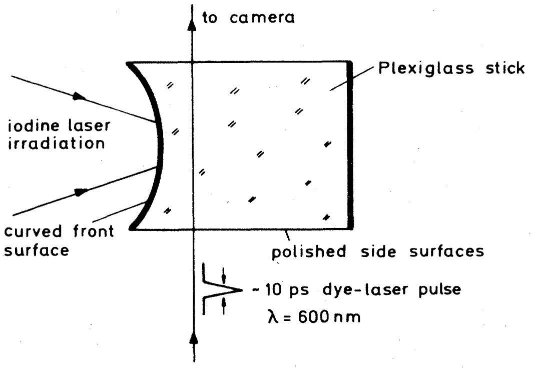

FIG. 1. Experimental arrangement.

The target consisted of a stick of Plexiglass [polymethylmethacrylate $(C_3O_2H_8)_n$] of 6×6 mm^2 cross section. Plexiglass was chosen because it has also been used in our previous studies and was readily available and easy to machine. A raw polish by hand was given to the surface of the stick, especially the side surfaces through which the shadowgraphy observations were made. The front surface was made slightly concave (radius 10 mm) in order to prevent diffraction at the edges of the target from disturbing the imaging of the vacuum-Plexiglass interface underneath the irradiated area. Note that internal total reflection of the dye-laser light from the curved surface causes the dark vertical band seen in the photographs. The plasma is hidden behind this dark band and, by reflection from the curved surface, its self-luminosity is partly suppressed.

The dye-laser system and the optical setup for imaging is described elsewhere in detail.[10] It consisted of an active-passively mode-locked, flashlamp-pumped dye laser and delivers a single ~10-ps pulse (wavelength $\lambda\cong600$ nm) at a time which could be set in advance relative to the iodine laser pulse. The target was imaged by an $f/10$ lens with a magnification of 12 onto Polaroid film. For each iodine laser shot one shadowgram could be obtained; the series of shadowgrams shown in Figs. 2 and 4 are thus composed from different events.

Quantitative measurements of shock-wave propagation were made with an electron streak camera (Imacon 600) with the streak slit parallel to the iodine-laser axis. For these measurements the dye laser was operated in the long-pulse mode (~1 μs pulse duration).

Figure 2 shows a series of shadowgrams taken at a laser intensity of 1.4×10^{14} W cm^{-2} (68 J, out of focus). Figure 2(a) is a control photograph taken before the iodine-laser shot; here it illustrates the interaction geometry. Note the nonuniformities in the dye-laser background illumination due to laser speckle and also the vertical scratches indicating imperfect polishing of the Plexiglass.

Figure 2(b) was taken 0.52 ns before the maximum of the iodine-laser pulse. At this time the vacuum-Plexiglass interface is still undisturbed. This indicates that the target is not affected by any prepulses from the iodine laser. Figures 2(c)—2(f) show the evolution of the shock wave with time up to 196 ns. The shape of the shock wave changes during this time interval from nearly planar to nearly hemispherical. Besides the main wave a slower planar wave is released throughout the field of view from the front surface; it is most apparent at late times [Figs. 2(d)—(f)]. It is a weak wave, traveling with the velocity of sound (3.1×10^5 cm s^{-1} in Plexiglass). Obviously, a (low-level) pressure pulse is generated over a large area around the focal spot (note that in the limit of a weak wave the propagation velocity approaches sound velocity and hence the wave strength cannot be determined from its velocity). Figure 2(g), taken after the shot, shows that permanent damage is left in the target. Inspection from the front side [Fig. 2(h)] shows that the damage is in the form of a crater.

A streak photograph taken under the same conditions (out of focus) as in Fig. 2 is shown in Fig. 3. In this photograph the phenomenon mentioned in the Introduction

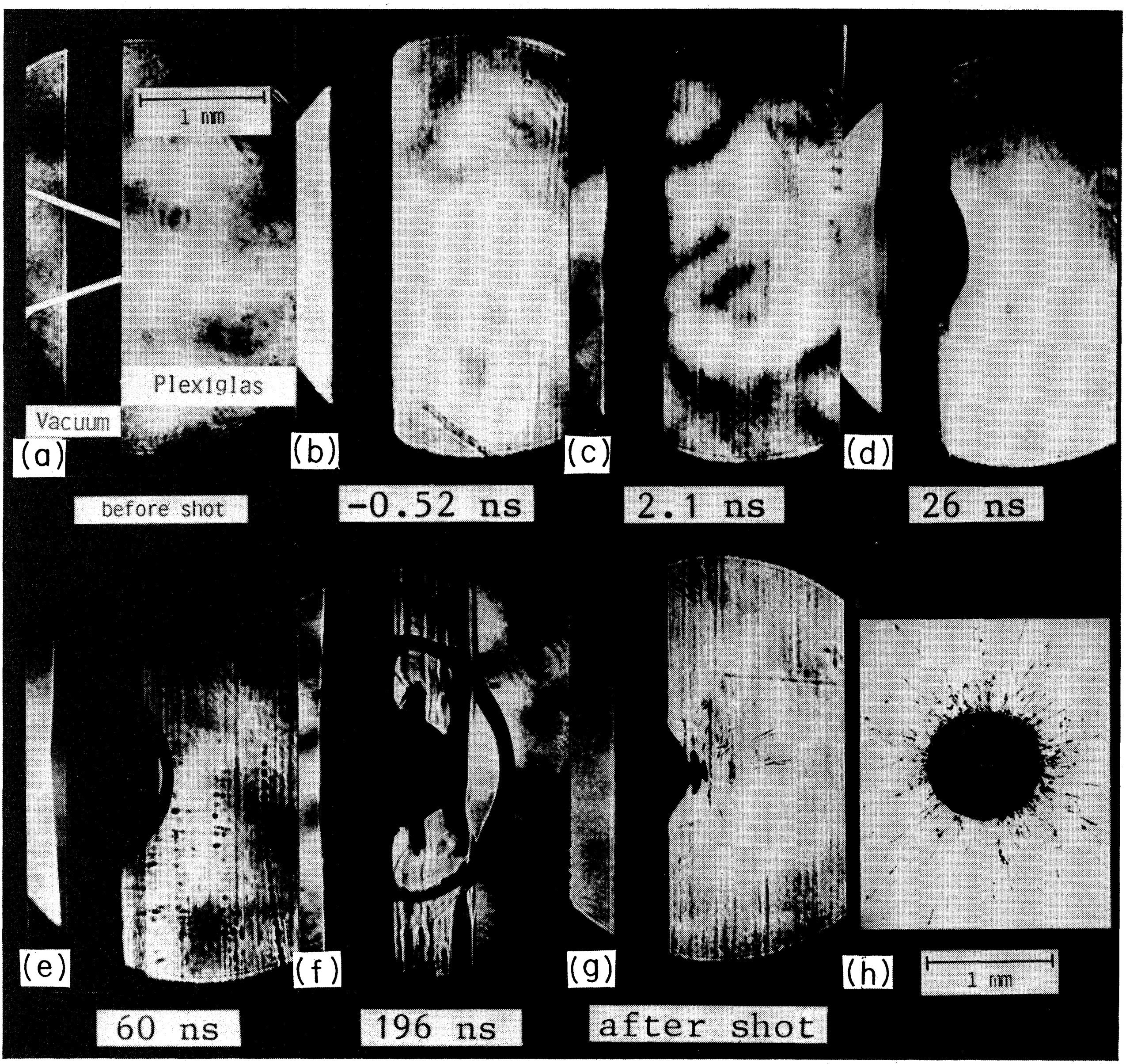

FIG. 2. Sequence of shadowgrams showing shock-wave propagation in Plexiglass at a laser irradiance of 1.4×10^{14} W cm^{-2}. (a) Illustration of interaction geometry. The vacuum-Plexiglass interface is at the right-hand edge of the dark vertical band. The picture was taken prior to a laser shot. (b) Undisturbed target immediately before the onset of the main laser pulse. (c)—(f) Shadowgrams showing the propagating shock waves. In the time interval 0—196 ns its shape changes from nearly planar to approximately hemispherical. (g) Permanent damage left in the target. (h) Front view of the crater in the target.

can be seen: during laser irradiation the Plexiglass suddenly becomes opaque to the dye-laser light. In Fig. 3, opaqueness sets in within a fraction of a nanosecond up to a depth of about $\sim$70 μm. Owing to this effect the shock wave cannot be seen for about 4 ns. The phenomenon itself and the cause of it are even better manifested in the shadowgrams taken at higher intensity as shown in Fig. 4 (this figure together with a short discussion of breakdown formed the subject of a previous short communication[11]).

Figure 4 shows a series of shadowgrams similar to Fig. 2 but now taken with the target in the in-focus position at $\Phi\cong3\times10^{15}$ W cm^{-2}. Figure 4(b) shows the Plexiglass interior 0.76 ns after the maximum of the iodine-laser pulse. A dark hemispherical cloud with diffuse boundaries has formed which is opaque to the dye-laser light. It extends about 500 μm into the Plexiglass. After 5.5 ns [Fig. 4(c)] treelike structures are now visible which extend from the interior of the dark cloud into the clear Plexiglass. These structures very much resemble the pattern of discharge channels found in corona discharges from a positive anode point.[12] We conclude from this similarity that what we observe here is basically an electrical breakdown phenomenon.

After 64 ns [Fig. 4(d)] the shock wave released from the

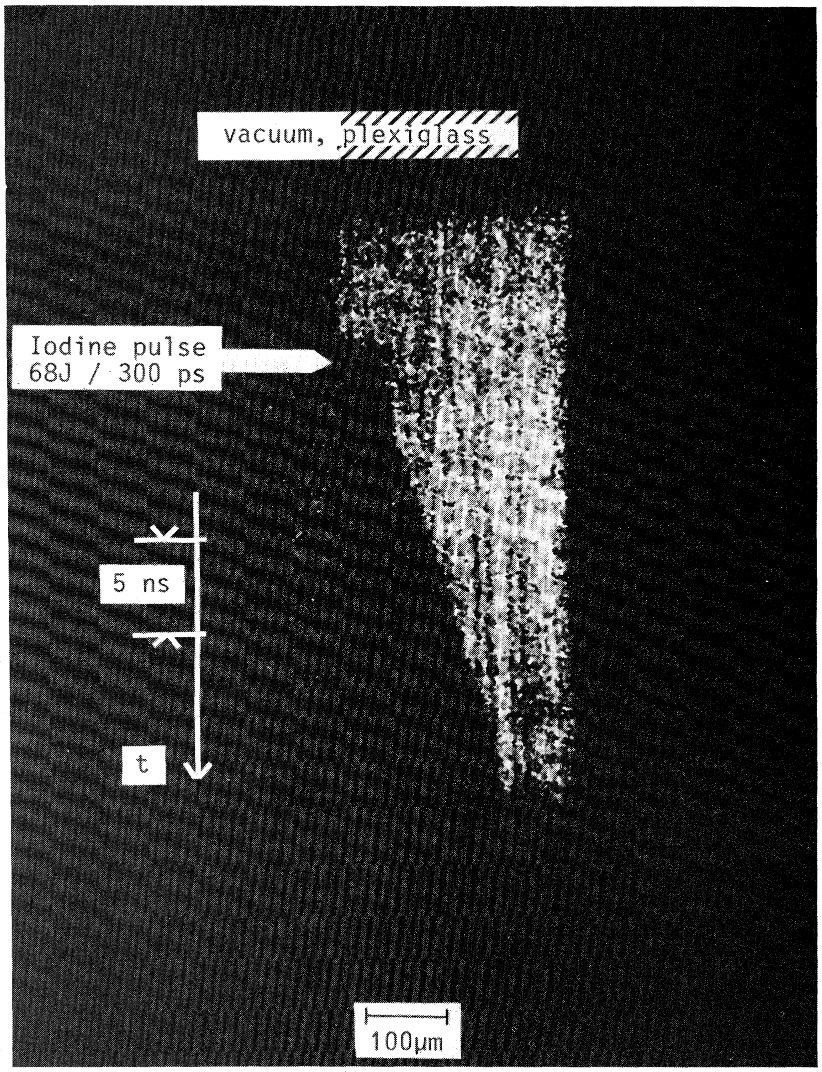

FIG. 3. Streak photograph (shadowgram) taken under similar conditions to those of the shadowgrams shown in Fig. 2. Note the higher magnification in comparison to Fig. 2.

irradiated area has caught up with the dimensions of the opaque cloud and becomes visible. At this late time the treelike structures do not grow further. However, numerous wavelets are released by them, indicating that energy has been deposited for the formation of these structures; the homogeneity of the material ahead of the shock front is thus disturbed. After 196 ns [Fig. 4(e)] the shock wave has proceeded further and separated from the opaque zone, but many disturbances are still visible in front of and behind the main front. In Figs. 4(d) and 4(e) one again sees the planar shock wave released along the target surface. Figure 4(f) shows the permanent damage to the target. In addition to the actual crater, brushlike structures are left in the deeper layers of the Plexiglass.

When the target is taken out of the vacuum chamber and inspected [Fig. 4(g), note the difference in magnification], surface damage with a starlike pattern is found around the irradiated area. The bright areas in Fig. 4(g) have become rough and scatter the illuminating light; dark areas are still polished and do not scatter. The damage traces bend around the stick and continue on the side surfaces. Figure 4(h) shows a magnified detail of Fig. 4(g), namely the crater left in the target surrounded by surface damage. Compared with Fig. 2(i), the crater seen in Fig. 4(h) is more regular. This is most likely due to the fact that with the target in the out-of-focus position the diameter of the irradiated area and the crater diameter are about equal, whereas in the in-focus position the irradiated area is much smaller than the crater diameter. The case of Fig. 4(h) is thus closer to a point explosion, where the shape of the crater becomes independent of the details of energy deposition. No streak photographs were taken under the conditions of Fig. 4 since it was clear that the shock wave could not be seen for the times of interest.

We note that an attempt was made to shield the interior of the target against breakdown by electroplating the whole Plexiglass stick with a 2-μm-thick copper layer. Only two small windows corresponding to the field of

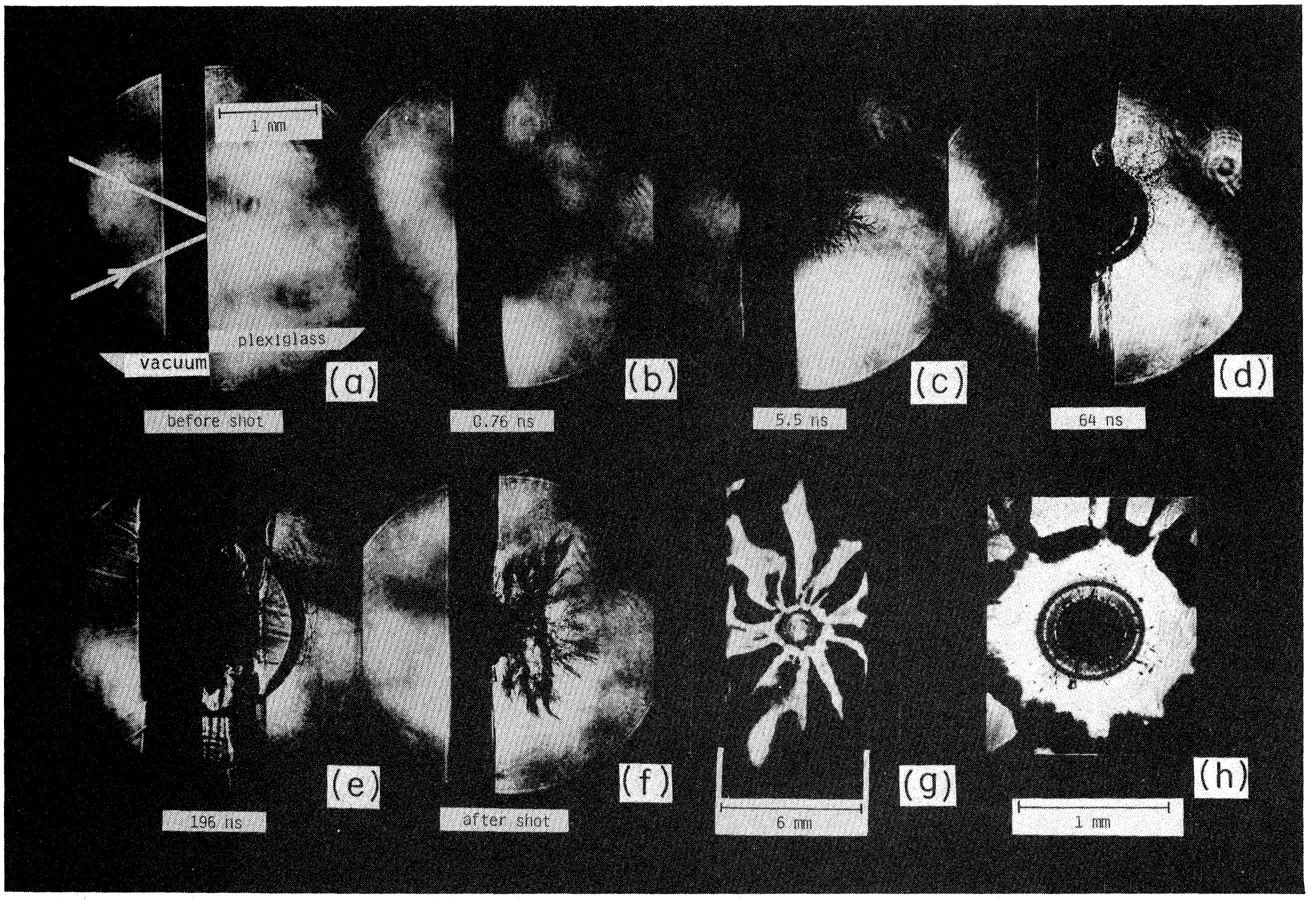

FIG. 4. Sequence of shadowgrams showing the internal breakdown of a Plexiglass target at a laser irradiance of 3×10^{15} W cm^{-2}. (a) Illustration of the interaction geometry. (b) Formation of a dark cloud. (c) Treelike discharge pattern. (d) and (e) Appearance of a hemispherical shockwave. (f) Permanent damage left in the target. (g) Starlike surface damage on the front side of the target. (h) Magnified detail of (g) showing laser-produced crater.

view of the shadowgraphy setup were left in the side surfaces of the target. The experiment, performed under in-focus conditions with the laser interacting with the copper layer, showed no significant reduction of the breakdown phenomenon.

III. ELECTRIC FIELD FORMATION AND TARGET BREAKDOWN IN THE PRESENCE OF TWO-DIMENSIONAL PLASMA EXPANSION

A. General remarks

Our observations revealed that breakdown in the target material obscures the initial phase of the shock-wave propagation, particularly for high laser intensities. Before we proceed to analyze the measured shock trajectories (as far as they could be observed), we discuss in this section the possible causes of breakdown in the target.

The laser irradiation generates a hot, expanding plasma in front of the irradiated surface. Owing to their low mass and high thermal velocity, the electrons tend to escape from the plasma, leaving behind a positive space charge and generating an electric field in the plasma. From the equation of motion for the electrons,[13] with electron inertia, magnetic fields, and momentum transfer from ions to electrons by collisions being neglected, the electric field is given by

$$\mathbf{E}=\nabla p_e/en_e \ . \tag{2}$$

Here p is the electron pressure, n_e the electron density, and e the elementary charge. In the following we shall show that the field leaking into the target is intense enough to explain the observed breakdown phenomenon and no other mechanisms have to be evoked. It is essential, however, to take the nonplanar character of the plasma expansion into account.

B. The electric field of a planar rarefaction wave

Let us discuss first the electric field formation in a planar, isothermal rarefaction wave, a model often used for the approximate description of a laser-produced plasma (see Fig. 5). In this model the irradiated surface is supposed to supply a stream of homogeneous plasma with a flow velocity equal to the sound velocity (i.e., Mach number $M=1$). The edge of the wave is thus kept stationary

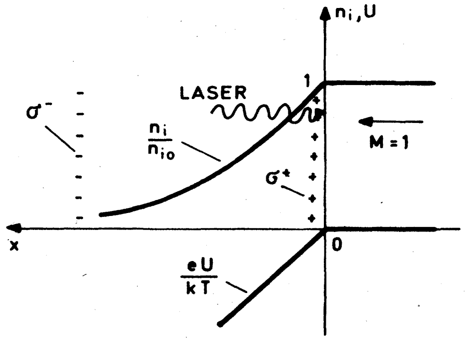

FIG. 5. Electric field generation in a planar rarefaction wave. U is the electric potential, M the Mach number.

in the laboratory frame. We assume a fully ionized plasma with ion mass m_i, ion charge Z, electron temperature T (the ions are assumed to be cold), electron density n, ion density n_i, and pressure $p = nkT$. It is assumed that the overall charge of the plasma is zero and expansion starts at $t = 0$. For the case of a neutral plasma with $n = Zn_i$ the density and pressure distribution in the expanding plasma for $t > 0$ are given by

$$n_i = p/ZkT = n_{i0}\exp(-x/st), \quad s^2 = ZkT/m_i \ . \tag{3}$$

Here s is the isothermal sound velocity. From Eq. (2) the electric field in the homogeneous part is zero; in the expansion region a spatially homogeneous electric field exists in the x direction, its amplitude being given by

$$E = kT/est \ . \tag{4}$$

This field is due to charge separation in the plasma. The location and magnitude of the space charges is readily found from Gauss's law. Because the field is discontinuous at $x = 0$, a positive (surface) charge is located at the edge of the wave, this being given by

$$\sigma = \epsilon_0 kT/est \ . \tag{5}$$

A negative charge of equal magnitude is located at the front of the wave. In the approximation of a neutral plasma it is located at $x = +\infty$ for $t > 0$. The front of the wave and the electric field thus spread out with infinite velocity in this approximation.

This unphysical feature is removed if allowance for charge separation is made and Poisson's equation is solved together with the equations of motion and continuity.[14] In this approximation the negative space charge is located near an ion front (a remnant of the discontinuity in the initial ion density distribution) which spreads out with finite velocity. Its approximate position can be estimated from the condition[15] that the gradient length $L = st$ of the expanding plasma becomes equal to the Debye length near the front. With this condition one obtains for the coordinate of the ion front

$$x_f \cong st\ln(\omega_{pi0}t) \ . \tag{6}$$

Here $\omega_{pi0} = (Z^2e^2n_{i0}/m_i\epsilon_0)^{1/2}$ is the ion plasma frequency corresponding to the initial plasma ion density n_{i0}. The positive and negative space charges are spread out by about a local Debye length but their magnitude is still given by Eq. (5).

C. The electric field of a plasma expanding in two dimensions

It is important to note that in planar geometry an electric field only exists in the space between the separated charges, i.e., in the inhomogeneous, expanding plasma. Outside this space the fields of the positive and negative charges cancel exactly. It is therefore not possible to understand the formation of an electric field in the homogeneous interior of the target, in a strictly planar model of plasma expansion.

Owing to the finite area of plasma production, however, the plasma expansion is two dimensional in reality [Fig. 6(a)]. As a result, the fields produced by the space charges do not cancel exactly and a "stray" field is generated outside the plasma, including the target interior.

For an order-of-magnitude estimate of the strength and time behavior of the field we assume in the following for the initial, quasiplanar phase of plasma expansions that the space charges are given by the planar rarefaction

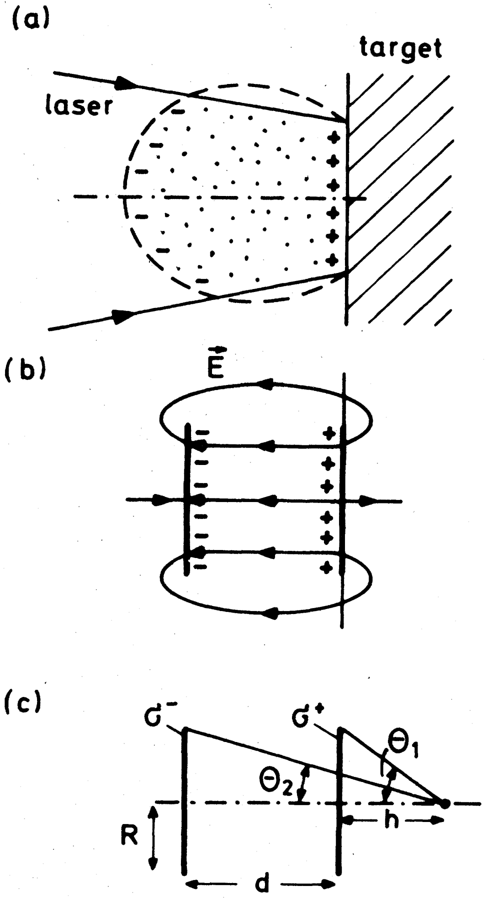

FIG. 6. Capacitor model for explaining electrical breakdown in the target. (a) Expansion of a plasma produced with a finite-size laser spot. (b) Capacitor model, illustrating the existence of a stray field in the interior of the target. (c) Notation for calculation of the fields.

model. The field is calculated in the model of a plate capacitor with circular plates [Fig. 6(b)]. The radius of the plates is taken as the plasma radius R, the distance and magnitude of the space charges are taken from the planar rarefaction model.

With the notations given in Fig. 6(c), the field on axis in the target interior is readily calculated as

$$E(\theta_1,\theta_2)=(\sigma/2\epsilon_0)(\cos\theta_2-\cos\theta_1)\ . \tag{7}$$

With the normalized coordinates $H=h/R$ and $D=d/R$ it can be written as

$$E(H,D)=(\sigma/2\epsilon_0)\{[1+(H+D)^{-2}]^{-1/2} -(1+H^{-2})^{-1/2}\}\ . \tag{8}$$

For $D \ll 1$ (i.e., $d \ll R$, small distance between plates) Eq. (8) may be expanded to give

$$E(H,\ D \ll 1)=(\sigma D/2\epsilon_0)(1+H^2)^{3/2}\ . \tag{9}$$

We are most interested in the field at $H=0$, i.e., immediately behind the irradiated spot. Inserting σ from Eq. (5) and $D=d/R \cong x_f/R$ using Eq. (6), one finds

$$E(H=0,\ D \ll 1)\cong -(kT/eR)\ln(\omega_{pi0}t)\ . \tag{10}$$

Compared with the field inside the expanding plasma [see Eq. (4)] the stray field inside the target is much weaker if one has $t \ll \tau_{\text{hydro}}/\ln(\omega_{pi0}t)$ (here we have introduced a characteristic hydrodynamic time $\tau_{\text{hydro}}=R/s$). The field varies only weakly (logarithmically) with time because the stray field enhancing effect of the increasing distance of the space charges is compensated by the field reducing effect of their temporal decay.

Equation (10) is approximately valid until x_f becomes of the order of the plasma diameter, i.e., until $x_f \cong 2R$ or, with Eq. (6), $t\ln(\omega_{pi0}t)=\tau_{\text{hydro}}$. Solving this implicit equation for t shows that the factor $\ln(\omega_{pi0}t)$ only depends very weakly on ω_{pi0} and τ_{hydro}. With ω_{pi0} in the range $10^{13}-10^{14}\ s^{-1}$ (i.e., n_{i0} in the range $10^{20}-10^{22}\ \text{cm}^{-3}$) and τ_{hydro} in the range $10^{-11}-10^{-9}$ s, the numerical value of $\ln(\omega_{pi0}t)$ only varies between 3 and 10. In the following we therefore always take $\ln(\omega_{pi0}t)=5$. Equation (10) is thus valid as long as $t \leq \tau_{\text{hydro}}/5$.

As expansion proceeds further, in the capacitor model the regime $D \gg 1$ (i.e., $d \gg R$, large distance between plates) is reached. Formally, one finds in this limit for $H=0$ from Eq. (8) and with Eq. (5),

$$E(H=0,\ D \gg 1)=-kT/2est. \tag{11}$$

Comparison with Eq. (4) shows that now the absolute values of the fields in the target and in the plasma are equal (the difference by a factor of 2 arises because the positive capacitor plate now carries field lines on both surfaces). This is a consequence of the fact that the negative charges are now far away and no longer produce a compensating field in the target interior. The decay of the field with t^{-1} [see Eq. (11)] suggested by the capacitor model is, however, unphysical because for $D \gg 1$ the assumption of planar expansion is no longer valid.

When the plasma expansion begins to exceed the source diameter, its character changes from the planar, nonstationary rarefaction wave to an approximately stationary flow (near the source). From the discussion above it seems plausible that in the stationary phase the field produced by the positive space charge is largely uncompensated and about equal to the field in the plasma itself. With this assumption it is possible to estimate the strength of the field in the stationary phase direct from Eq. (2), assuming a characteristic length L for the density gradient, i.e.,

$$E \cong -kT/eL. \tag{12}$$

There is a certain ambiguity about the choice of L. Depending on whether one assumes that the plasma becomes stationary at $t \cong \tau_{\text{hydro}}/\ln(\omega_{pi0}t)$ (corresponding to the condition $x_f \cong 2R$) or at $t=\tau_{\text{hydro}}$ (corresponding to $st \cong 2R$), one calculates from Eq. (3) $L=R/\ln(\omega_{pi0}t)$ or $L=R$, respectively. We leave it open which estimate is the better one; the difference is not large, however, because $\ln(\omega_{pi0}t) \leq 10$, as noted above.

The result of our considerations is then that the electric field in the target is always in the range

$$kT/eR \leq E \leq kT\ \ln(\omega_{pi0}t)/eR\ , \tag{13}$$

in the initial nonstationary phase [Eq. (10)] as well as in the later, stationary phase of plasma expansion [Eq. (12)]. The field is determined by the electron temperature in the expanding plasma and the radius of the area over which plasma is produced. The time dependence of the field is very weak if T and R remain constant.

We note that in Ref. 11 we considered the plasma as a conducting sphere of radius R, charged to a potential U and with a field $E=U/R$ at its surface (causing breakdown). The model discussed here gives some more insight into the physical processes, especially into the temporal evolution of the field, but is otherwise obviously identical in spirit. The potential U is found here to be of the order $U=kT/e$ [possibly enhanced by a factor $\ln(\omega_{pi0}t)$].

D. Application to the experimental results

With the target in focus (i.e., at high laser intensity) it is well known that so-called hot electrons are generated during laser-target interaction whose temperature will determine the magnitude of the electric field. With $kT \cong 25$ keV in this case[8] and $R \cong 50\ \mu\text{m}$ one obtains from Eq. (13)

$$5\times10^8 \leq E \leq 2.5\times10^9\ \text{V/m}\ .$$

These fields are of the same order of magnitude as the breakdown fields of dielectric materials (10^8-10^9 V/m); breakdown in the target is thus indeed expected under in-focus conditions. Propagation of the breakdown phenomenon into regions of lower field strength possibly leads to the observed self-termination of the phenomenon at a depth of $\cong 500\ \mu\text{m}$.

With the target out of focus, the generated field should be weaker for two reasons. Firstly the plasma radius is larger ($R \cong 250\ \mu\text{m}$) and secondly the hot-electron temperature smaller, about 8 keV. For the out-of-focus conditions one might expect therefore that the field is a factor of about 20 weaker and breakdown is near its threshold or even absent. Careful inspection of the shadowgrams shows that in this case breakdown is localized at individual points of the irradiated area. It seems possible that at these points local disturbances such as scratches, dust grains on the target surface, or localized plasma phenomena lead to field enhancement and local breakdown. This leaves some hope that in experiments performed under cleaner conditions breakdown may be avoided for intensities of around 10^{14} W cm^{-2}.

As concerns the possibility of shielding the target interior with a conducting surface layer, we note that the characteristic frequency of the electric field variation is of the order of $\omega \cong 2\pi\tau_L^{-1}$. The skin depth $\delta = (2\epsilon_0 c^2/\sigma\omega)^{1/2}$ for copper [low-frequency conductivity $\sigma = 5.67\times10^7$ (Ω m)$^{-1}$] is $\delta = 1.2\times10^{-4}$ cm for $\tau_L = 300$ ps. It is therefore not surprising that the electric field could not be shielded with a copper layer of about this same thickness. It should be kept in mind that with the application of (even thicker) shielding layers impedance-matching problems between the two materials have to be faced.

In concluding our discussion of the breakdown phenomenon it should be emphasized that our model considerations, taking only electrostatic features into account, considerably simplify the situation. It is well known from experiment[16–18] and simulation[19] that not only electric fields but also intense magnetic fields are generated in the expanding plasma. The magnetic field modifies electron transport and leads in particular to a spreading of fast electrons along the target surface. Corresponding observations[16,17] have been made in CO_2-laser irradiations as well as in the present experiment.[18]

Under in-focus conditions we observed previously[18] that fast electrons deposit a fraction of about 15% of the absorbed energy in a ringlike area with a diameter of several millimeters surrounding the focal spot. It is possible that some of the observations made during the course of this experiment are related to this lateral spreading of fast electrons. The energy deposition by fast electrons may lead to the planar wave released from the target surface throughout the field of view (note that for this weak wave the propagation velocity is nearly equal to the sound velocity and therefore not very dependent on local variations of the density of energy deposition). Another observation, namely the starlike damage traces seen in Fig. 4(g), may have to do with the fact that the fast electrons deposit also electric charge. As a consequence an outward-propagating surface breakdown may be generated leading to the observed surface damage. It is clear that these phenomena are complex and need further investigation.

In our simplified treatment of internal breakdown the existence of fast electrons is taken into account through the hot-electron temperature but the additional complications of magnetic-field-induced lateral spreading are ignored. This seems justified insofar as formation of intense electric fields due to charge separation in the two-dimensionally expanding plasma appears unavoidable and should not be affected, at least in order of magnitude, by the simultaneous generation of magnetic fields. As it can explain the breakdown phenomenon there is no need for more complicated (or even "anomalous") explanations. As we noted above, some of the observed effects may well be connected with the generation of magnetic fields and their effect on transport. But these occur in regions of low energy density with no obvious connection to the focal area where the breakdown phenomenon under discussion is centered.

IV. COMPARISON OF MEASURED AND CALCULATED SHOCK-WAVE TRAJECTORIES

After the shock front has traversed the opaque breakdown zone its motion can be measured by framing and streak photography and compared with calculated shock-wave trajectories. For our discussion let us divide the generation and decay of the shock wave into three consecutive phases.

The first phase is during laser irradiation when a hot plasma is generated at the irradiated surface. The recoil momentum of the expanding plasma drives a shock wave in the opposite direction, i.e., into the dense target material. It is important that the characteristic densities for the plasma and shock-wave regions are quite different. For the plasma region the characteristic density is the critical density ρ_c (equal to 2.2×10^{-3} g cm^{-3} at the iodine laser wavelength in a fully ionized material); for the shock-wave region it is the solid density ρ_0 (equal to 1.18 g cm^{-3} for Plexiglass). A consequence of this difference in density is that only a small fraction of the absorbed energy is transferred to the shock-wave region. This is readily seen from the laws of momentum and energy conservation which, in the stationary regime, are approximately

$$\rho_c s^2 \cong \rho_0 s_0^2 , \tag{14}$$

$$\Phi_{\text{abs}} \cong \rho_c s^3 . \tag{15}$$

Here the flow velocities have been taken of the order of the sound velocities in the two regions (denoted by s and s_0, respectively, in the plasma and shock-wave regions). The ratio of the convective fluxes, corresponding to the fractional energy transfer to the shock-wave region, is of the order of $\rho_0 s_0^3/\rho_c s^3 \cong (\rho_c/\rho_0)^{1/2} \cong 0.04$. From momentum conservation the ratio of the flow velocities is of the same order, namely $s_0/s \cong (\rho_c/\rho_0)^{1/2}$, i.e., the shock-wave velocity is much smaller than the velocity of the expanding plasma. The latter is given approximately by $s \cong (\Phi_{\text{abs}}/\rho_c)^{1/3}$; for example, with $\Phi_{\text{abs}} = 10^{14}$ W cm^{-2}, one finds $s \cong 8\times10^7$ cm s^{-1}.

The second phase begins after the end of the laser pulse when the laser-produced plasma disappears. At this time a layer of dense, compressed material exists underneath the original target surface, bounded by a shock front towards the target interior and by a region with a steep density gradient towards the vacuum. When the pressure exerted during the first phase on the compressed layer by the laser-produced plasma suddenly ceases, the compressed material begins to expand freely into the vacuum. A rarefaction wave overtakes and attenuates the shock wave with time. The hydrodynamic flow during this second phase corresponds to the motion of a gas under the action of an impulsive load as discussed in the book of Zel'dovich and Raizer[20] (see Chap. XII). The flow approaches with time a self-similar solution where x_f, the coordinate of the shock front, is given by

$$x_f = At^\alpha \cong (\Pi_1/\rho_0)^{1/2}\tau^{1-\alpha}t^\alpha \ . \qquad (16)$$

The pressure amplitude Π_1 and the time constant τ characterize the applied pressure pulse (the exact numerical value of the constant A depends on the shape of the pressure pulse). The exponent α depends on the adiabatic index γ; for example, for $\gamma = \frac{5}{3}$, one has $\alpha = 0.611$ (in planar geometry). Note that this exponent is somewhat lower than the value $\alpha = \frac{2}{3}$ corresponding to a planar explosion in an infinite medium. The more rapid attenuation of the shock wave is due to the outflow of gas into the vacuum.

So far we have tacitly assumed that a planar shock wave is generated in the target. However, because the pressure pulse is applied over a finite area, it is clear that after a time when the shock front has moved a distance of the order of the radius of the affected area, a third phase begins. In this phase the hydrodynamic flow approaches more and more that of a concentrated (pointlike) rather than a planar impact. The exponent α then decreases and approaches a value below but close to $\frac{2}{5}$, this corresponding to a point explosion in an infinite medium. This means that the shock front slows down more rapidly than in the preceding phase (we note that an approximate treatment is given in Ref. 20). Below we shall make use of two-dimensional computer calculations for the simulation of this phase.

Let us now discuss the experiments performed with the larger spot diameter (out of focus). Using the approximate formulas given above, one estimates that during irradiation the plasma expands a distance of about 300 μm, i.e., comparable to the radius of the irradiated area. The flow during the first phase may thus be considered as planar. During the second phase the planar flow is maintained for about 5 ns. The flow of the shock-compressed material is therefore still approximately planar when the shock front becomes observable in the experiment. At later times the shock front will attenuate more rapidly than predicted for planar geometry.

The experiments with the larger spot diameter were simulated with our one-dimensional Lagrangian hydrodynamic LAPLAS code.[21] In its latest version this code uses the SESAME equation of state.[22] Unfortunately, the equation of state of Plexiglass is not contained in this library; the data of another plastic polyurethane, were thus used instead. The initial density was chosen as $\rho_0 = 1.18$ g cm^{-3}, corresponding to the density of Plexiglass. For comparison, an ideal-gas equation of state was used as well.

The code results are shown in Figs. 7 and 8. The pressure p behind the shock front, the compression ratio $\rho_{\max}/\rho_0$, and the coordinate of the shock front x_f are shown as functions of time in Fig. 7 during the first 5 ns. A peak pressure of $\sim$6 Mbar is reached during irradiation which subsequently decreases.

As Fig. 8 shows, the shock travels somewhat faster in a material of realistic equation of state than in an ideal gas. This is a consequence of the fact that the real material is less compressible than the ideal gas. For example, after 20 ns the compression ratio is $\rho_{\max}/\rho_0 \simeq 2$, whereas for the ideal gas it is still near its limiting value $\rho_{\max}/\rho_0 = 4$. The fact that, for a given pressure, the shock travels faster in a less compressible material may be seen from the general relation (1). We note that a more detailed discussion of equation-of-state effects on the behavior of a laser-irradiated target has been given in Ref. 23 with particular emphasis on laser-irradiated foils. Self-similar solutions for the plane impulsive-load problem including a Mie-Grüneisen equation of state are given in Ref. 24.

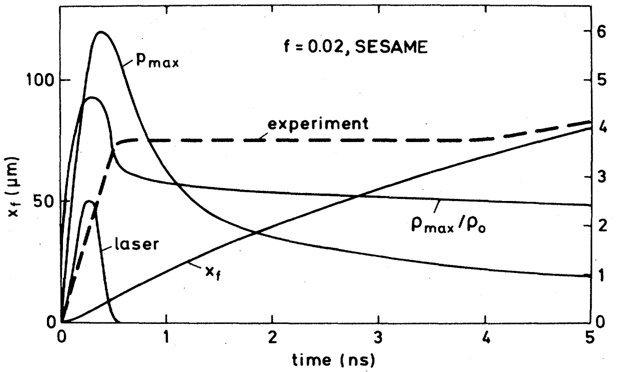

FIG. 7. Comparison of one-dimensional simulation of shock propagation with experiment. x_f is the shock-front position, p the pressure, $\rho_{\max}/\rho_0$ the compression ratio of the shock wave; in addition, the laser intensity is shown. A flux limiter $f = 0.02$ and the SESAME equation of state were used. The first 4 ns are obscured by the breakdown phenomenon.

In comparing simulation and experiment it must be kept in mind that the calculated shock trajectory depends on several parameters, in particular the absorbed laser energy E_{abs}, the laser pulse duration τ_L, the radius R of the heated area, and the flux limiter f for electron heat conduction. The concept of flux limitation which models phenomenologically complex transport phenomena[25] is chosen because it is simple and affords a quantitative description of plane foil acceleration experiments.[8] The accuracy with which these parameters are known is relavant for assessing the agreement of simulation and experiment.

Taking into account the proportionalities $\Pi \sim \Phi^{2/3}$, $\Phi \sim E_{\text{abs}}\tau_L^{-1}R^{-2}$, $\Pi \sim f^{0.16}$ (from Ref. 8), one finds from

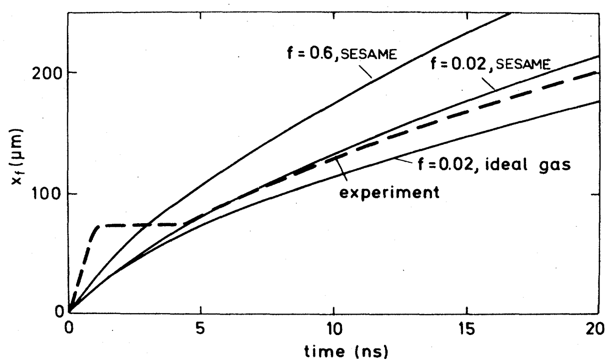

FIG. 8. Comparison of a measured shock-front trajectory (Fig. 3) with one-dimensional simulations using different equations of state and flux limiters.

Eq. (16) that $x_f \sim E_{\rm abs}^{1/3} \tau_L^{-1/3} R^{-2/3} f^{0.08}$. The absorbed energy is calculated from the incident energy (measured in each shot) on the basis of averaged data of previous absorption measurements.[8] For the pulse duration a mean value of 280($\pm$60) ps determined by streak camera measurements is used. The numerical value of the flux limiter ($f=0.02$) was taken as in previous simulations of thin-film experiments.[8] Because x_f only depends weakly on $E_{\rm abs}$ and τ_L and even less on f, the largest uncertainty comes from the value of R. It was taken equal to the radius of the optical spot, with the possibility of enlargement due to lateral conduction being ignored. The input data for the simulations contain no other free parameter.

The experimentally measured shock trajectory is hidden up to $\cong 4$ ns by the breakdown phenomenon. When it becomes visible, it agrees rather well with the trajectory where flux limitation and the equation of state are taken into account. The ideal-gas calculation gives a somewhat lower and the calculation without flux limitation ($f=0.6$) a somewhat larger propagation distance than measured.

In view of the uncertainties in the experimental conditions, the good agreement between experiment and simulation appears somewhat fortuitous. Nevertheless, it is quite satisfactory that agreement is obtained for the same choice of parameters which previously resulted in a proper simulation of thin-foil experiments.[8]

Comparing the numerical simulations with the self-similar behavior [Eq. (16)], we find that for $t \geq 2$ ns the computed shock-front position follows a power law $x_f \sim t^{\alpha}$; α agrees with theoretical predictions within 2% (Ref. 20, $\alpha=0.61$ for $\gamma=\frac{5}{3}$ ideal gas).

In the experiments with the small irradiation area (in focus) the characteristic distance of plasma expansion of about 700 μm is much larger than the radius of the irradiated area. Hence the plasma flow during the first phase is already two dimensional. The second phase is completely obscured by the breakdown phenomenon. When the shock front becomes visible ($t \geq 60$ ns), it is long in the third phase and is hemispherical in shape.

The in-focus experiments at 3×10^{15} W cm^{-2} on an 85-μm-diam focal spot were simulated with the two-dimensional Eulerian POLLUX code, which uses quasi-Lagrangian rezoning.[26] The SESAME equation of state is included. The mesh size was 100×40 points in axial and radial directions, respectively. Again, $f=0.02$ was adopted. Figure 9 shows a density contour plot at 64 ns together with the corresponding velocity field. In this plot, the density varies between $\rho_{\rm min}=0.06$ g/cm^3 and $\rho_{\rm max}=2.2$ g/cm^3. The 20 contour lines are equally spaced on a logarithmic scale, i.e., from one to the next line the density increases by the factor 1.2. The velocity is related linearly to the length of the arrows; the largest velocity arrow corresponds to 6×10^5 cm/sec. The initial target thickness was 600 μm. This plot is to be compared with Fig. 4(d) keeping in mind that the scales in the axial and transverse directions of the plot are different.

With the help of the two-dimensional code a study about the influence of various parameters on the shock-wave trajectory was made. The following parameters were considered.

(i) *Equation of state.* The shock-wave trajectory was computed for the SESAME and ideal-gas equation of state; the result is shown in Fig. 10. For the ideal gas the initial temperature was chosen such that the sound velocity in the undisturbed material matches the sound velocity in Plexiglass. As in the one-dimensional case the more realistic SESAME equation of state gives a somewhat higher velocity but the difference is slight. Note that the experimental point in Fig. 10 was obtained from Fig. 4(d).

(ii) *Diameter of the area of energy deposition.* A comparison of the calculated and measured shape of the shock front allows us to establish limits for the size of the area of energy deposition. If it is made equal to the optical spot size, the calculations (see Fig. 9) show that the shock front has a bowl-like shape with a width-to-depth ratio (measured from the intersection point of laser axis and target surface) of 0.9. As discussed in Ref. 20 this is due to the attenuation of the wave by expansion of material along the free surface. The experiment, on the other hand [see Fig. 4(d)], shows a perfectly hemispherical shape with less than 5% deviation from sphericity. Varying the diameter of the area of energy deposition in the calculations showed that for a diameter of 200 μm a hemispherical shock wave was generated as observed in the experiment. This may be an indication that the area of energy deposition is somewhat enlarged compared to the optical spot size; such an enlargement has been in-

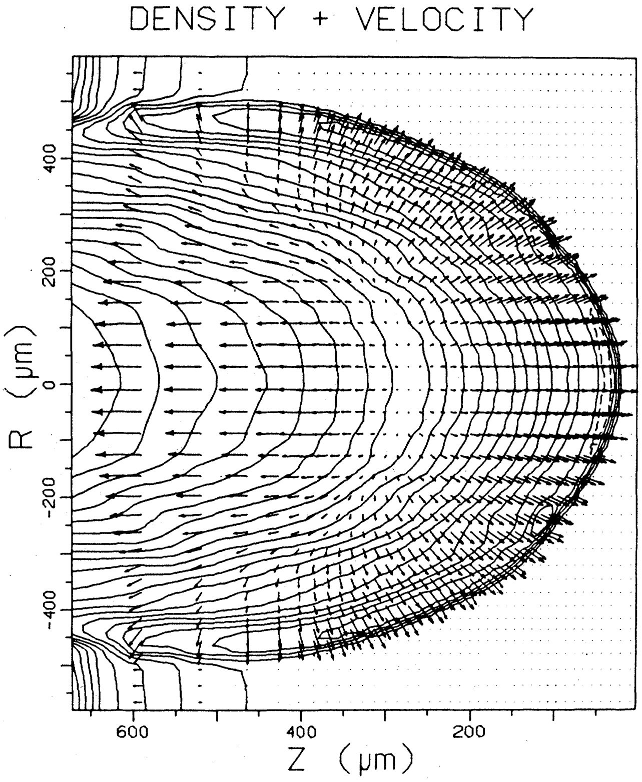

FIG. 9. Two-dimensional simulation of the in-focus experiment at 3×10^{15} W cm^{-2} irradiance. Isodensity contours (logarithmic scale, 20 steps from 0.06—2.2 g/cm^3) and velocity arrows (linear scale, longest arrow is 6×10^5 cm/s) are given at $t=64$ ns.

ferred from other observations in Ref. 27. However, it seems unlikely that the enlargement significantly exceeds 200 μm. This is concluded from the experiments with the 450-μm-diam focal spot size. With such a large spot (see Fig. 2) the width-to-depth ratio of the wave clearly exceeds 1 for the whole observation time up to 196 ns [Fig. 2(f)]. In order to investigate also the effect of the size of the deposition area on the shock-wave trajectory, its diameter was arbitrarily enlarged 4 times (i.e., 340-μm diameter) in some runs, keeping the total absorbed energy constant. As is seen in Fig. 10, for the larger area of energy deposition the shock lags behind initially (because of the reduced laser intensity and pressure) but catches up with the nominal case later (because the planarity of the shock is preserved for a longer time). No difference is left at the time of the experiment (64 ns). Obviously, the initial conditions become "forgotten" with time (in a similar way as in a point explosion[20]) and cannot be recovered in a unique manner from a measurement of the shock position at late time alone.

(iii) *Effective absorbed energy.* The absorbed energy is measured rather accurately in the experiment, but a fraction of it could be transported away (for example by fast electrons and ions or discharge phenomena) to much larger distances than is characteristic for the processes under investigation. The planar wave released along the target surface shows that long-range energy transport exists in principle; also, recent shock-wave studies[28] show some evidence that these losses may be energetically significant. In order to obtain bounds for this effect we have reduced the absorbed energy to $\frac{1}{4}$ of its nominal value in some calculations. The calculated shock-wave trajectory (see Fig. 10) differs too much from the experimental point at 64 ns, i.e., such a large reduction of the effective absorbed energy is not consistent with the experiment (a reduction by a factor of 2 at most cannot be excluded with the present experimental accuracy). We cannot confirm therefore (at least for our experimental conditions) the much more drastic reductions in the effective energy found in Ref. 28.

As we noted already, it is not possible to reconstruct the initial conditions unambiguously for the in-focus experiments. In particular, the peak pressure during irradiation remains quite uncertain. For the nominal conditions the simulations indicate 50 Mbar. If we assume an effective spot radius of twice the nominal one, the peak pressure drops to 20 Mbar. If we allow simultaneously a spot size enlargement to 200 μm and an energy reduction to one-half, the pressure reaches only 10 Mbar. According to the simulations, these differences in the initial conditions affect the shock-wave propagation not strong enough to be distinguished experimentally after 64 ns.

Finally, it is interesting to compare the simulation results with self-similar models. Inspection of Fig. 10 shows that for $t \geq 10$ ns the calculated shock-wave trajectory (on axis) is well described by a power law $x_f \sim t^{\alpha}$ with $\alpha \simeq 0.4$. As expected, this value of α is close to that obtained for a strong point explosion.[20] Unfortunately, the accuracy of the two-dimensional simulations is not sufficient to resolve a definite difference. For late times, the shock wave ceases to be strong, especially in the lower-energy case. Then the self-similar description breaks down according to its "intermediate asymptotic" range of validity.[29] This can be seen in the code results by a deviation of the calculated shock trajectory from the self-similar prediction for a strong wave.

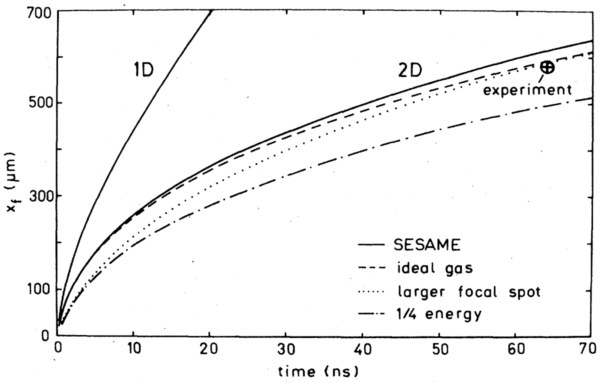

FIG. 10. Shock-front position vs time from two-dimensional simulations. Solid and dashed lines show SESAME and ideal-gas equations of state, respectively. Dotted line: focal spot diameter increased by a factor of 4. Dash-dotted line: input energy reduced by a factor of 4. For comparison, a one-dimensional simulation is added. Experimental point was obtained from Fig. 4(d).

V. SUMMARY AND CONCLUSIONS

Laser-induced shock-wave propagation in Plexiglass was observed by optical shadowgraphy. Two cases were investigated:

(i) an out-of-focus experiment with a 450-μm diameter of the irradiated area and a laser intensity of 1.4×10^{14} W cm^{-2},

(ii) an in-focus experiment with an 85-μm diameter of the irradiated area and a laser intensity of 3×10^{15} W cm^{-2}.

The shock wave generated in the out-of-focus experiment with the relatively large spot diameter remains approximately planar for a time of the order of 10^{-8} s. One-dimensional simulations of the shock-wave trajectory suggest a peak pressure of 6 Mbar during irradiation.

In the in-focus experiments the hydrodynamic motion of the heated material is nonplanar from the very beginning. As a consequence of the fact that the observation time begins rather late (64 ns) the initial conditions cannot be recovered unambiguously, initial peak pressures of 10—50 Mbar being consistent with the observations. It is possible, however, to infer limits for the size of the area and the amount of energy deposition.

It is satisfactory that the present shock-wave experiments could be successfully simulated with the same input data as previous thin-foil acceleration experiments.

The experimental investigation also showed a hitherto unknown phenomenon, namely, electrical breakdown in the Plexiglass layers underneath the irradiated area (up to a depth of $\sim$0.5 mm) and indications of surface breakdown in the vicinity of the laser spot (up to a distance of several mm). In the breakdown volume the Plexiglass became opaque, impeding observation of the shock-wave trajectory for 4 ns (out-of-focus experiments) and 60 ns (in-focus experiments). In addition, energy deposition in the breakdown channels disturbs the homogeneity of the material.

The generation of intense electric fields and the associated breakdown phenomena should be taken seriously as a possible limitation of the potential of laser-induced pressure waves as a quantitative tool of high-pressure physics. A discussion of the phenomenon shows that fields of the order of $E \cong kT/eR$ are generated by charge separation during two-dimensional expansion of the laser-heated plasma. These fields are high enough to explain the observed phenomena. To reduce these fields, large laser spots, i.e., powerful lasers, are required (the temperature and hence laser intensity have to be maintained in order to achieve the derived pressures). The laser illumination and target surface should also be uniform in order to avoid local breakdown effects. With the laser used for our investigations (100-J, 300-ps pulses) it may be possible to avoid breakdown at intensities up to 10^{14} W cm^{-2}, i.e., pressures below about 10 Mbar, but this has to be confirmed by additional experiments.

ACKNOWLEDGMENTS

The authors wish to thank G. J. Pert for making available his two-dimensional code POLLUX, and K. Eidmann and S. Witkowski for discussions and critical reading of the manuscript. This work was supported in part by the Commission of the European Communities in the framework of the Association Euratom—Max-Planck-Institut für Plasmaphysik.

---

[*] Permanent address: Ecole Polytechnique, F-91128 Palaiseau, France.

[†] Permanent address: Department of Electrical Engineering, University of Alberta, Edmonton, Alberta, Canada T6G 2G7.

[‡] Permanent address: Shanghai Institute of Laser Technology, 319 Yueyang Road, Shanghai, China.

[1] *Physics of High Energy Density, Proceedings of the International School of Physics "Enrico Fermi" Course XLVIII,* edited by P. Caldirola and H. Knoepfel (Academic, New York, 1971).

[2] C. G. M. van Kessel and R. Sigel, Phys. Rev. Lett. 33, 1020 (1974).

[3] C. G. M. van Kessel, Z. Naturforsch. **30a**, 1581 (1975).

[4] D. Billon, D. Cognard, J. Lanuspach, C. Paton, D. Redon, and D. Schirman, Opt. Commun. **15**, 108 (1975).

[5] L. R. Veeser and J. C. Solem, Phys. Rev. Lett. **40**, 1391 (1978).

[6] R. J. Trainor, J. W. Shaner, J. M. Auerbach, and N. C. Holmes, Phys. Rev. Lett. **42**, 1154 (1979).

[7] F. Cottet, J. P. Romain, R. Fabbro, and B. Faral, Phys. Rev. Lett. **52**, 1884 (1984).

[8] K. Eidmann, F. Amiranoff, R. Fedosejevs, A. G. M. Maaswinkel, R. Petsch, R. Sigel, G. Spindler, Yung-lu Teng, G. Tsakiris, and S. Witkowski, Phys. Rev. A **30**, 2568 (1984).

[9] G. Brederlow, E. Fill, and K. J. Witte, *The High-Power Iodine Laser* (Springer, Berlin, 1983); see also G. Brederlow, R. Brodmann, K. Eidmann, A. Krause, M. Nippus, R. Petsch, R. Volk, S. Witkowski, and K. J. Witte, Projektgruppe für Laserforschung, Garching, Report No. PLF-5, 1979 (unpublished).

[10] Y. L. Teng, R. Fedosejevs, and R. Sigel, Max-Planck-Institut für Quantenoptik, Garching, Report No. MPQ-43, 1981 (unpublished).

[11] R. Fedosejevs, Yung-lu Teng, R. Sigel, K. Eidmann, and R. Petsch, J. Appl. Phys. **52**, 4186 (1981).

[12] E. Nasser, *Fundamentals of Gaseous Ionizaton and Plasma Electronics* (Wiley, New York, 1971).

[13] S. I. Braginskii, in *Reviews of Plasma Physics,* edited by M. A. Leontovich (Consultants Bureau, New York, 1965), Vol. 1.

[14] J. E. Crow, P. L. Auer, and J. E. Allen, J. Plasma Phys. **14**, 65 (1975).

[15] J. S. Pearlman and R. L. Morse, Phys. Rev. Lett. **40**, 1652 (1978).

[16] P. A. Jaanimagi, N. A. Ebrahim, N. H. Burnett, and C. Joshi, Appl. Phys. Lett. **38**, 734 (1981).

[17] M. A. Yates, D. B. van Hulsteyn, H. Rutkowski, G. Kyrala, and J. U. Brackbill, Phys. Rev. Lett. **49**, 1702 (1982).

[18] F. Amiranoff, K. Eidmann, R. Sigel, R. Fedosejevs, A. Maaswinkel, Yungl-lu Teng, J. D. Kilkenny, J. D. Hares, D. K. Bradley, B. J. MacGowan, and T. J. Goldsack, J. Phys. D **15**, 2463 (1982).

[19] D. W. Forslund and J. U. Brackbill, Phys. Rev. Lett. **48**, 1614 (1982).

[20] Ya. B. Zel'dovich and Yu. P. Raizer, *Physics of Shock Waves and High-Temperature Hydrodynamic Phenomena* (Academic, New York, 1967).

[21] R. F. Schmalz, P. Mulser, and G. Spindler, Max-Planck-Institut für Quantenoptik, Garching, Report No. MPQ-75, 1983 (unpublished).

[22] B. I. Bennet, J. D. Johnson, G. I. Kerley, and G. T. Rood, Los Alamos National Laboratory Report No. LA-7130, 1978 (unpublished).

[23] R. F. Schmalz and J. Meyer-ter-Vehn, Phys. Fluids **28**, 932 (1985).

[24] S. I. Anisimov and V. A. Kravchenko, Z. Naturforsch. **40a**, 8 (1985).

[25] J. P. Matte, T. W. Johnston, J. Delettrez, and R. L. McCrory, Phys. Rev. Lett. **53**, 1461 (1984).

[26] G. J. Pert, J. Comput. Phys. **49**, 1 (1983).

[27] M. H. Key, W. T. Toner, T. J. Goldsack, J. D. Kilkenny, S. A Veats, P. F. Cunningham, and C. L. S. Lewis, Phys. Fluids **26**, 2011 (1983).

[28] F. Cottet, J. P. Romain, R. Fabbro, and B. Faral, J. Appl. Phys. **55**, 4125, (1984).

[29] G. I. Barenblatt, *Similarity, Self-Similarity, and Intermediate Asymptotics* (Consultants Bureau, New York, 1979).

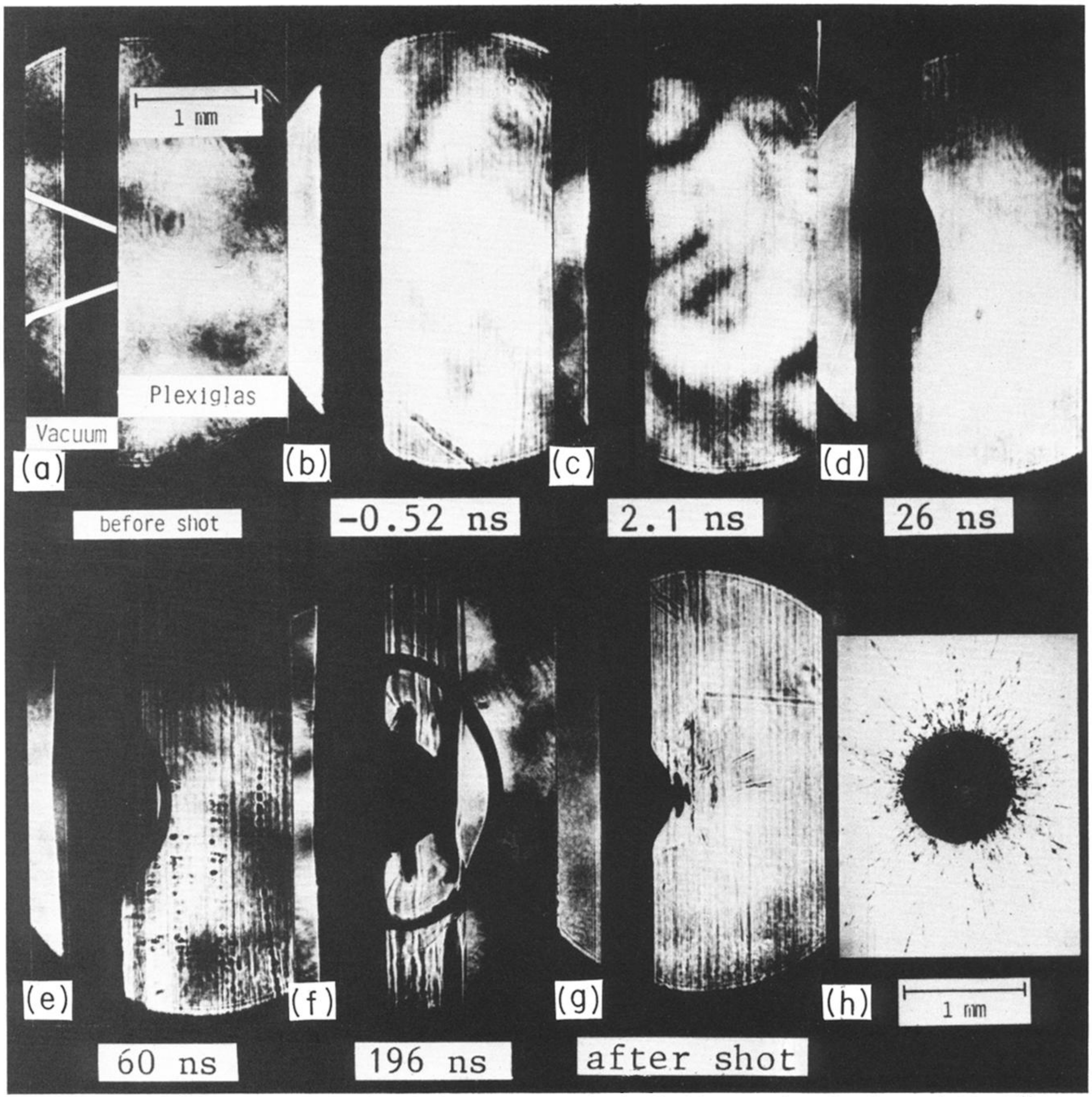

FIG. 2. Sequence of shadowgrams showing shock-wave propagation in Plexiglass at a laser irradiance of 1.4×10^{14} W cm^{-2}. (a) Illustration of interaction geometry. The vacuum-Plexiglass interface is at the right-hand edge of the dark vertical band. The picture was taken prior to a laser shot. (b) Undisturbed target immediately before the onset of the main laser pulse. (c)—(f) Shadowgrams showing the propagating shock waves. In the time interval 0—196 ns its shape changes from nearly planar to approximately hemispherical. (g) Permanent damage left in the target. (h) Front view of the crater in the target.

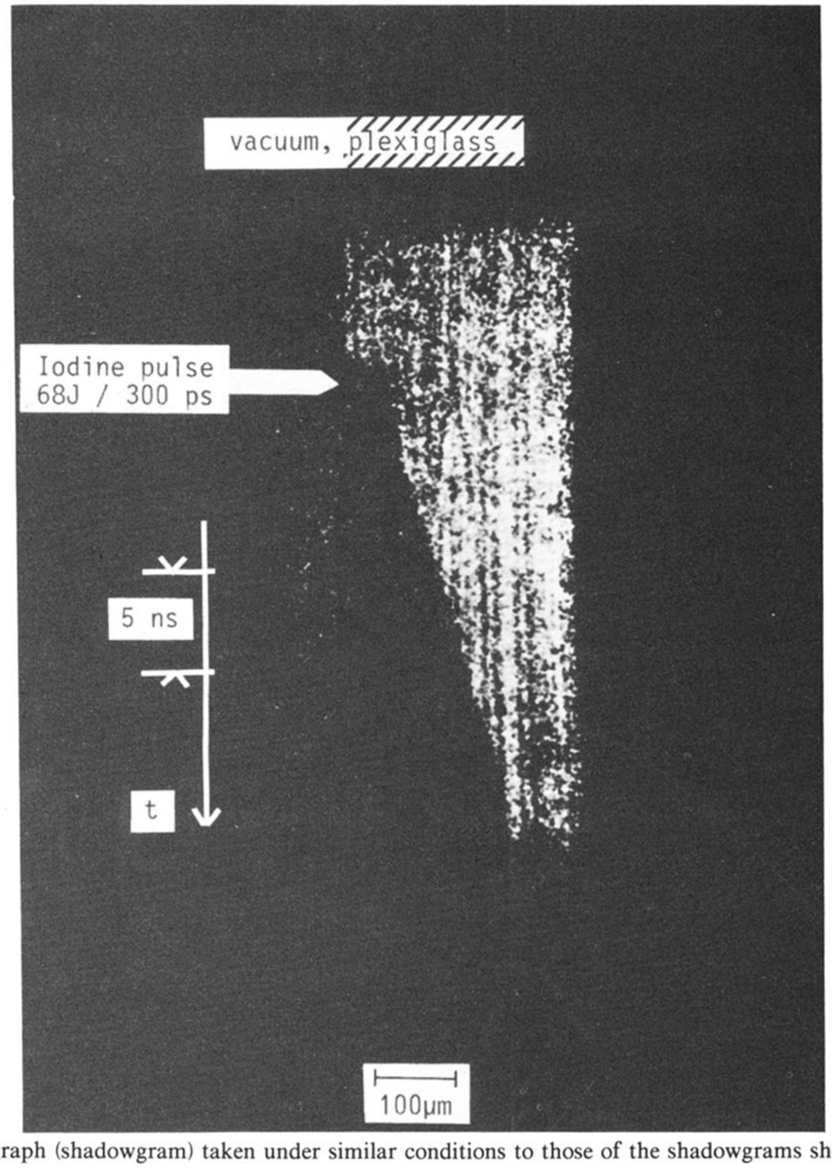

FIG. 3. Streak photograph (shadowgram) taken under similar conditions to those of the shadowgrams shown in Fig. 2. Note the higher magnification in comparison to Fig. 2.

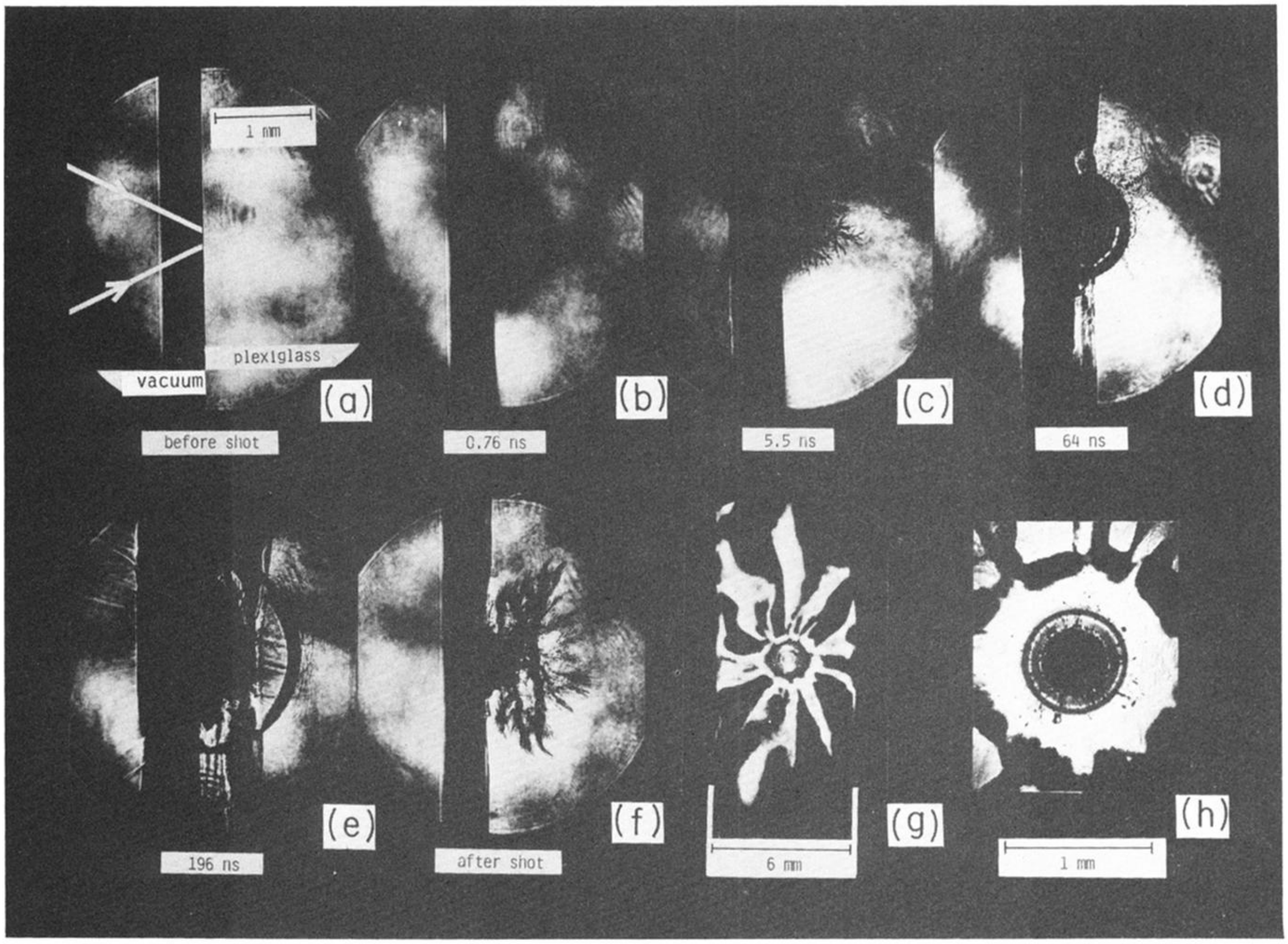

FIG. 4. Sequence of shadowgrams showing the internal breakdown of a Plexiglass target at a laser irradiance of 3×10^{15} W cm^{-2}. (a) Illustration of the interaction geometry. (b) Formation of a dark cloud. (c) Treelike discharge pattern. (d) and (e) Appearance of a hemispherical shockwave. (f) Permanent damage left in the target. (g) Starlike surface damage on the front side of the target. (h) Magnified detail of (g) showing laser-produced crater.